ON THE FORMATION OF DEFECT CLUSTERS IN MC SILICON SOLAR CELLS

Dietmar Kohler, Annika Zuschlag, Sven Seren, Giso Hahn
University of Konstanz, Department of Physics, P.O. Box X916, 78457 Konstanz, Germany
Phone: +49 (0) 7531 88 3174, Fax: +49 (0) 7531 88 3895, Email: dietmar.kohler@uni-konstanz.de

ABSTRACT: Defect clusters in multicrystalline silicon can have a strong influence on the quality of the material and the resulting solar cells. In this work we present an experimental approach to a better understanding of the formation of two huge defect clusters. We explore large quantities of wafers and solar cells from the same brick. This enables us to find the lateral and vertical positions where the formation of the clusters starts during crystallization. Measurements of these solar cells including light-beam induced current (LBIC), optical scans and microscope images of grain-selective etched wafers allow for a closer look. They are compared to EBSD measurements that provide information about the grain boundary types as well as the grain orientations in this location. This offers a better understanding of the cluster formation.
Keywords: Defects, Grain, Multicrystalline Silicon

1 INTRODUCTION

Defect clusters are local accumulations of defects. These defects are grain boundaries and especially dislocations, which can be caused by thermal stress during crystallization. The influence of these defects on the material quality and – in association with this – on solar cells depends on several factors, e.g. their decoration with impurities [1-4].

In an earlier publication, we presented results that small solar cells, which were cut out of larger area cells with large dislocation clusters, showed a local decrease in open circuit voltage and especially in short circuit current density for solar cells with a homogenous emitter [5]. But not all small sample solar cells with non-radiative recombination-active defect clusters showed the same behavior. It could be assumed that the observed effects were caused by the defect clusters as well as large area networks of defects. In this work, we take a closer look on the origin and the formation of two defect clusters.

A large quantity of wafers from the same brick was available for this experiment. This allowed the identification of the lateral and vertical positions of the clusters' origin of formation. Some of the wafers were processed to solar cells and were measured with a forward bias electroluminescence setup. The parts of neighboring wafers that contained the cluster formation areas were cut into 2 x 2 cm^2 pieces and were polishing etched. Then, the exact positions of the cluster origins were measured with electron back-scatter diffraction (EBSD) to receive information about the crystal orientation as well as the grain boundary types.
Other neighboring wafers were etched in an alkaline solution and then scanned using an optical scanner setup to receive optical information about the crystal structure.

2 MATERIAL & SOLAR CELL PROCESS

The studied material was part of a compensated p-type multicrystalline silicon ingot. The 12.5 x 12.5 cm^2 wafers came from different heights in a typical brick. About half of the brick's wafers were available. For this study, some of them were selected with focus on the formation of two defect clusters.

Some of the wafers were processed to solar cells with a homogenous emitter and screen-printed firing through SiN_x metallization. Neighboring wafers were cut into small pieces and chemical polishing (CP) etched with an etching solution based on hydrofluoric acid, acetic acid and nitric acid.

Other wafers were alkaline etched in order to enhance the reflection contrast between crystal grains of different orientations.

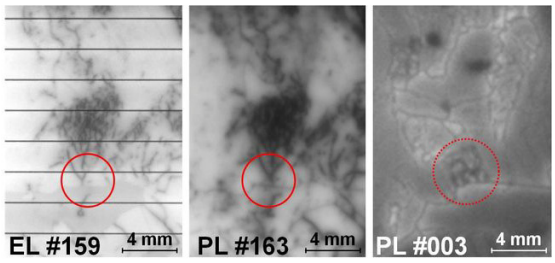

Figure 1: Electroluminescence (EL) and photoluminescence (PL) measurements of a defect cluster region. The clustering already started at the bottom of the ingot (right). At the marked areas, the defects seem to grow in contact with the large grain beneath.

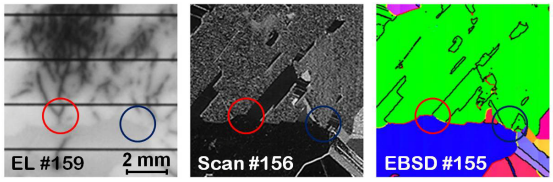

Figure 2: Close-up pictures of the cluster area in Fig. 1. The circles mark areas where the defects grow further for higher positions. The optical scanning of a grain-selective etched wafer (middle) and EBSD (right) indicates that the defects grow in a [101] oriented grain (in green) at a grain boundary with the large [111] grain (in blue) beneath.

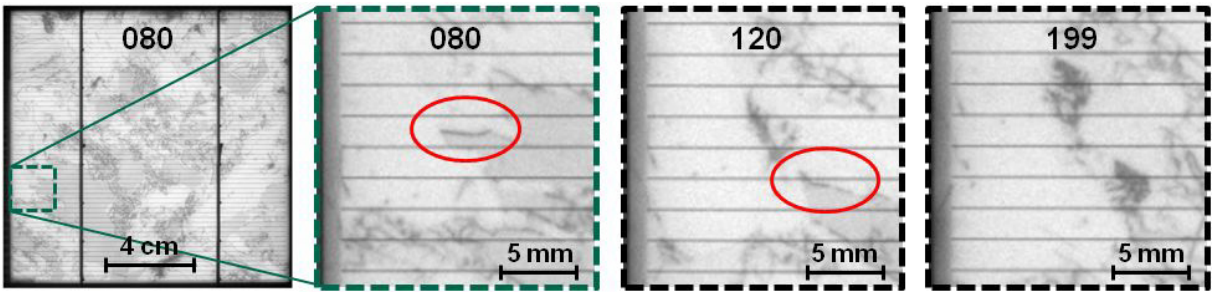

Figure 3: Electroluminescence images under forward bias from solar cells from different heights show the formation of two small defect clusters at a grain boundary. The red marked boundary is investigated in Fig. 4 and Fig. 5.

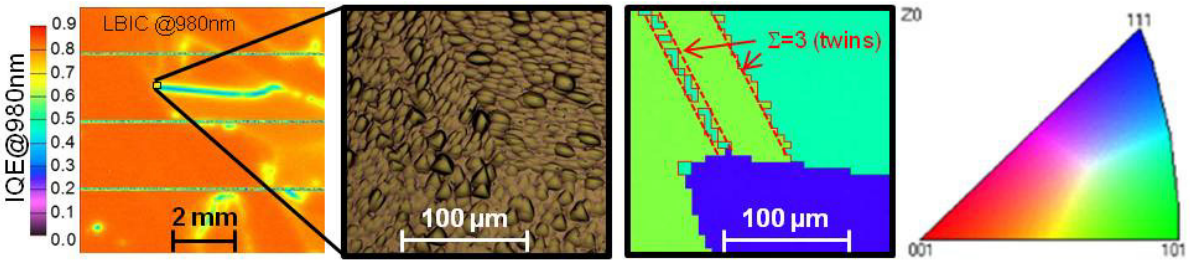

Figure 4: The location at the height position #080, where a defect cluster comes to formation, imaged by means of LBIC, optical microscope and EBSD.

3 CHARACTERIZATION

The solar cells were characterized with electroluminescence (EL) under forward bias as well as light-beam induced current (LBIC).

The alkaline etched wafers were scanned with a fast optical scanner at a relatively low resolution to receive rough reflection maps. The acidic polishing etched wafers were imaged with an optical microscope. Additionally, we took a closer look to a selection of wafer pieces using a scanning electron microscope (SEM). When the probe is placed in an angle of about 70 degrees, some of the back-scattered electrons can lead to diffraction patterns. These Kikuchi patterns of this EBSD measurement contain information on the symmetry, the orientations and the relative angles of the crystal grains. This allows the determination of the grain orientations and grain boundary types in the observed area [6,7]. The maps in this work show superpositions of orientation maps – based on inverse pole figure (IPF) – and the grain boundary types according to coincidence site lattices.

4 RESULTS AND DISCUSSION

In the material that was used in this experiment, three defect clusters exceeded a horizontal dimension of 1 cm^2 and grew up to several cm^2. Two of these clusters are presented in this work. In Fig. 1, two different states of the first cluster can be seen. In the luminescence images of #159 and #163, a part of the large defect cluster is visible as dark pattern. The cluster contains defects that are strongly recombination active for minority charge carriers. This explains also the decrease of the minority charge carrier lifetime that can be seen in the PL image of the full SiN_x passivated #163. These influences are similar to those of singular dislocations and grain boundaries and are commonly known. The impact of the defect clusters depends on the dislocation density as well as the success of the gettering and passivation processes [1,8]. The cluster parts in Fig. 1 are all connected to a large grain boundary that can be seen below the cluster. This is also the case for #003 from the bottom of the ingot. By comparing several luminescence measurements from several positions, the formation of this cluster can be traced back to this lowest available position. Therefore this is an example for a defect cluster that started close to the crucible bottom at the beginning of the crystallisation. The connection of this cluster to the large grain boundary is clearly visible in Fig. 2. This is in accordance with several results that stresses at certain grain boundaries tend to be reduced by dislocations [9,10].

As the EBSD measurement shows no grain boundary at this position, these connections might be formed by lineages of dislocations. The step size of 25 µm might involve not-detected twins, but those typically show a rather low recombination activity due to the high symmetry and therefore low decoration. For higher positions, the connections continue to grow while the recombination active defects in the grain with [101] direction (in green) seem to be shifted away from the grain in [111] direction (in blue). This effect can be caused by a higher growth rate of this grain as the growth velocity of different grains depends on the grain orientation as well as the crystallisation rate [11].

Fig. 3 shows the EL images of forward biased solar cells from different heights of the ingot. The formation of two defect clusters can be seen. For the height position #198, both clusters are clearly visible, indicating a rather large loss due to non-radiative recombination. For the lower position #120, only the upper cluster is visible while the second cluster is just starting to grow, close to a significant grain boundary. For the even lower position #080, only this grain boundary is visible. The measurements of neighboring wafers show that the upper cluster here is about to grow very close to the left end of the grain boundary. Therefore, we took a closer look at this location. The LBIC measurement on the left side in

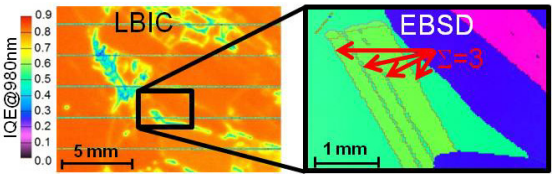

Figure 5: The doubled twin boundaries are also presumed to be the cause for the formation of a second defect cluster near position around #120 (LBIC, EBSD).

Fig. 4 illustrates the loss in the internal quantum efficiency (IQE) at this grain boundary, while other grain boundaries in this region show nearly no effect. The strong loss can be explained by an assumed high decoration of the grain boundary with impurities. We focussed on the region of interest concerning the formation of the two defect clusters. The brownish image in Fig. 4 was made by optical microscopy and shows the surface at this location. The oval or triangular structures are the results of the acidic CP etching and reveal the same orientations of these surface structures on a small scale and different orientations for neighboring areas in the upper right corner. At least two parallel diagonal changes of orientation can be distinguished in this section.

The different orientations can be seen as well in the EBSD measurement (Fig. 4c) which provides information about the distinct grain orientation. The combination of the grain orientations and the Euler angles of neighboring grains allows for the determination of the type of the enclosed grain boundary. All visible diagonal grain boundaries are Σ3 grain boundaries. This might indicate that this region underwent strong stress during crystallization [12]. The diagonal line close to the tip of the grain marked in dark blue even consists of doubled Σ3 grain boundaries right next to each other. So, if this interpretation is correct, stress might have occured at the place where these grain boundaries cross with the recombination-active grain boundary at the bottom of the image. Therefore, the formation of the defect cluster probably started at this location. But it is difficult to determine the causalities. An alternative explanation is that the twin boundaries as well as the defect clusters are both related to and brought forward by the present [101] orientation.

Also for this cluster, the neighboring grain orientation is [111]. This orientation is expected to be dominant for crystallisation rates below 30 µm/s (=10.8 mm/h) in mc Si because of a higher growth rate due to a lower interface energy [11,13,14].

The same effects were observed for the formation of a second defect cluster that follows up at position #120 as shown in Fig. 5. Here, several paired twin grain boundaries can be seen in the EBSD measurement while the first cluster is shifted upwards along the diagonal grain boundary.

An exemplary image showing the disappearing of a defect cluster can be seen in Fig. 6. The scan image on the left side indicates a bent grain boundary between two grains with very different reflection which means different crystal orientations. The LBIC measurement shows that the right one of these two grains contains a large defect cluster. EL measurements from lower heights revealed that this cluster was formed from the merge of the two grown clusters mentioned above.

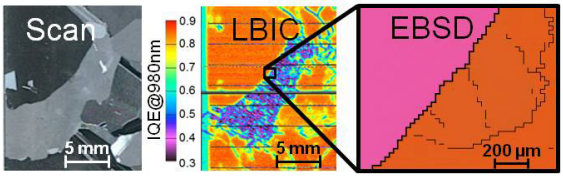

Figure 6: At position #419, both observed and united defect clusters finally end by shifting into a stable large grain boundary as shown in these measurements by optical scan, LBIC and EBSD.

The small sub-grain boundaries in EBSD in the defect cluster on the right side of the grain boundary disappear while the whole cluster is shifted towards the boundary of the large grain on the left side.

5 SUMMARY & OUTLOOK

Defect clusters can have a relevant influence on the open circuit voltage and the short circuit current density due to non-radiative recombination. This is why we took a closer look at the formation of two defect clusters. One cluster already started at the bottom of the ingot and grew along a grain boundary inside a [101] grain. The clusters seemed to start close to a grain boundary with decreased internal quantum efficiency – which is probably caused by a high decoration with impurities. EBSD measurements showed that the very location contains Σ3 twin boundaries that lie close to each other. The stress during crystallisation that might have been related with the close twin boundaries is one explanation for the formation of defect clusters at this location. But it is definitely hard to distinguish between causality and coincidence of the observed grain boundaries in this case. More likely is that the twins as well as the cluster might be caused by the specific present grain orientations. Both large clusters grow in grains in [101] direction at a grain boundary with a stable [111] oriented grain.

In this work, we interpreted only the results for two cluster areas. For a reliable and more general conclusion it is necessary to investigate further areas with large defect clusters.

6 ACKNOWLEDGEMENTS

The financial support from the BMU project FKZ 0325079 is gratefully acknowledged in particular for the processing equipment. The content of this publication is the responsibility of the authors.

REFERENCES

[1] B.L. Sopori, *Defect Clusters in Silicon: Impact on the Performance of Large-Area Devices*, Materials Science Forum 258–263 (1997) 527.

[2] B. Sopori, V. Budhraja, P. Rupnowski, S. Johnston, N. Call, H. Moutinho, M. Al-Jassim, *Defect clusters in multicrystalline silicon: Their nature and influence on the solar cell performance*, Proc. 34th IEEE PVSC (2009) , 001969.

[3] M.M. Kivambe, G. Stokkan, T. Ervik, B. Ryningen, O. Lohne, *The microstructure of dislocation clusters in industrial directionally solidified multicrystalline*

silicon, Journal of Applied Physics 110(6) (2011) 063524.

[4] S. Martinuzzi, I. Périchaud, F. Warchol, *Hydrogen passivation of defects in multicrystalline silicon solar cells*, Solar Energy Materials and Solar Cells 80(3) (2003) 343.

[5] D. Kohler, D. Kiliani, B. Raabe, S. Seren, G. Hahn, *Comparison of UMG materials: Are ingot height independent solar cell efficiencies possible?*, Proc. 25th EU PVSEC (2010) 2542.

[6] G.E. Lloyd, *Atomic number and crystallographic contrast images with the SEM : a review of backscattered electron techniques*, Mineralogical Magazine 51 (1987).

[7] A. Zuschlag, H. Morhenn, J. Bernhard, J. Junge, S. Seren, G. Hahn, *Microscopic analysis of the influence of solar cell process steps on the recombination activity of extended crystal defects*, Proc. 25th EU PVSEC (2010) 2433.

[8] M. Rinio, H.J. Möller, M. Werner, *LBIC Investigations of the Lifetime Degradation by Extended Defects in Multicrystalline Solar Silicon*, Solid State Phenomena, 63–64 (1998) 115.

[9] D. Hull, D.J. Bacon, *Introduction to Dislocations*, 5th ed. Elsevier Ltd (2011).

[10] B. Ryningen, G. Stokkan, M. Kivambe, T. Ervik, O. Lohne, *Growth of dislocation clusters during directional solidification of multicrystalline silicon ingots*, Acta Materialia, 59(20) (2011), 7703.

[11] K. Fujiwara, Y. Obinata, T. Ujihara, N. Usami, G. Sazaki, K. Nakajima, *Grain growth behaviors of polycrystalline silicon during melt growth processes*, Journal of Crystal Growth, 266(4) (2004) 441.

[12] T. Ervik, M. Kivambe, G. Stokkan, B. Ryningen, O. Lohne, *Dislocation formation at Σ=27a boundaries in multicrystalline silicon for solar cells*, Proc. 26th EU PVSEC (2011) 1895.

[13] B. Ryningen, *Formation and growth of crystal defects in directionally solidified multicrystalline silicon for solar cells*, PhD Thesis, NTNU, 2008.

[14] K. Fujiwara, K. Nakajima, T. Ujihara, N. Usami, G. Sazaki, H. Hasegawa, S. Mizoguchi, K. Nakajima, *In situ observations of crystal growth behavior of silicon melt*, Journal of Crystal Growth, 243(2) (2002) 275.